
Fully Steerable 3D Spherical Neurons

Pavlo Melnyk, Michael Felsberg, Mårten Wadenbäck

Computer Vision Laboratory, Department of Electrical Engineering, Linköping University
 {pavlo.melnyk, michael.felsberg, marten.wadenback}@liu.se

Abstract

Emerging from low-level vision theory, steerable filters found their counterpart in deep learning. Earlier works used the steering theorems and presented convolutional networks equivariant to rigid transformations. In our work, we propose a steerable feed-forward learning-based approach that consists of spherical decision surfaces and operates on point clouds. Due to the inherent geometric 3D structure of our theory, we derive a 3D steerability constraint for its atomic parts, the hypersphere neurons. Exploiting the rotational equivariance, we show how the model parameters are fully steerable at inference time. The proposed spherical filter banks enable to make equivariant and, after online optimization, invariant class predictions for known synthetic point sets in unknown orientations.

1 Introduction

In this paper, we present a steerable feed-forward model for point cloud classification, an important and challenging problem with many applications such as autonomous vehicles, human-robot interaction, and mixed-reality installations. The steerability is achieved by fully steerable geometric neurons, leading to a rotation equivariant network. Besides becoming a geometrically explainable approach, further benefits are rotation invariant classification using a simple online optimization during inference and reduced data augmentation requirements during learning.

While the vast majority of works on steerable models, which we review in Section 2, use convolutional neural networks (CNNs) as the base architecture, we focus on rotations only. However, the proposed feed-forward network can easily be expanded into a CNN to cover 3D rigid body motions.

In our work, we make use of a conformal embedding to obtain higher-order decision surfaces and show how a spherical classifier, i.e., the hypersphere neuron [1, 2, 3] or its generalization for input point sets — the geometric neuron [4] — can be turned into a steerable neuron, when input data is in 3D. We show that the aforementioned spherical neurons in both 2D and 3D require only first-order spherical harmonics to accommodate the effect of rotation. This enables us to derive a 3D steerability constraint for the spherical neurons and to describe a recipe to create a steerable model from a pretrained spherical classifier.

Using the synthetic Tetris dataset [5], we first verify the derived constraint and check its stability with respect to perturbations in the input. Next, we conduct an experiment in a realistic setting, where we initialize the steerable model parameters using a noisy prediction of the transformation applied to the input and optimize the parameters in an unsupervised way.

The focus of our work is on how understanding the geometry of spherical neurons enables implementing the powerful theoretical concepts of steerability and equivariance, i.e., the theoretical derivation and the geometric intuition. Thus, the accompanying experiments provide empirical evidence on a conceptual level, and future large scale experiments on real-world data are expected to be essential for applications of our theory.

The contributions of our work are as follows:

- (a) We derive a 3D steerability constraint for spherical neurons based on a minimal set of four spherical classifiers that are rotated to the corresponding vertices of a regular tetrahedron (Section 3.1.1).
- (b) We propose a method to turn a trained spherical classifier into a fully steerable model (Section 3.1.3) according to (a) that produces predictions equivariant to 3D rotations, even in the presence of noise.
- (c) We propose an unsupervised optimization procedure (Section 4.4) applied at inference time that determines the 3D rotation from noisy predictions and show how the obtained steerable model can produce invariant class predictions for a synthetic point set.

2 Background

2.1 Steerable filters

As per [6], a 2D function $f(x, y)$ is said to steer if it can be written as a linear combination of rotated versions of itself, i.e., when it satisfies the constraint

$$f^\theta(x, y) = \sum_{j=1}^M v_j(\theta) f^{\theta_j}(x, y), \quad (1)$$

where $v_j(\theta)$ are the interpolation functions, θ_j are the basis function orientations, and M is the number of basis function terms required to steer the function. An alternative formulation can be found in [7]. In 3D, the steering equation becomes

$$f^{\mathbf{R}}(x, y, z) = \sum_{j=1}^M v_j(\mathbf{R}) f^{\mathbf{R}_j}(x, y, z), \quad (2)$$

where $f^{\mathbf{R}}(x, y, z)$ is $f(x, y, z)$ rotated by $\mathbf{R} \in \text{SO}(3)$, and each $\mathbf{R}_j \in \text{SO}(3)$ orients the corresponding j th basis function.

Theorems 1, 2 and 4 in [6] describe the conditions under which the steerability constraints (1) and (2) hold, and how to determine the minimum number of basis functions for the 2D and 3D case, respectively.

2.2 Equivariant models

Geometric equivariance has been an object of extensive research over the last decades [8]. In [9], Lie theory is used to study steerable filters for equivariance and invariance. Equivariance is a necessary property for steerability as the group acting on the input space needs to be represented in the co-domain of the operator. Nowadays, equivariance-related research extends into deep learning, e.g., the $\text{SE}(3)$ -equivariant model [5] and the $\text{SO}(3)$ -equivariant network [10], as well as [11, 12].

The use of steerable filter concepts is also a noticeable trend in this type of works. For example, the work of [13] considers image data and proposes a new CNN architecture to produce equivariant representations with steerable features, which involve fewer parameters than traditional CNNs. They consider the dihedral group (rotation, translation and reflection), and the steerable representations in their work are proposed as formation of elementary feature types. One limitation of their approach is that rotations are restricted to four orientations, i.e., by $\pi/2$. More recently, [14] utilized group convolutions and introduced steerable filter convolutional neural networks (SFCNNs) operating on images to jointly attain equivariance under translations and discrete rotations. In their work, the filter banks are learned rather than fixed. The work of [15] proposes a unified framework for $\text{E}(2)$ -equivariant steerable CNNs and presents their general theory.

Closer related to our work in terms of the type of data are CNNs for 3D data proposed in [16]. The authors employed a combination of scalar, vector and tensor fields as features transformed by $\text{SO}(3)$ representations and presented a model that is equivariant to $\text{SE}(3)$ transformations. They also considered different types of nonlinearities suitable for non-scalar components of the feature space.

Unlike the recent works, we focus on feed-forward models with building blocks derived by means of conformal (geometric) algebras [17].

2.3 Conformal embedding

The utility of conformal embedding for Euclidean geometry and the close connection to Minkowski spaces are thoroughly discussed in [17]. The Minkowski $\mathbb{R}^{1,1}$ plane with orthonormal basis defined as $\{e_+, e_-\}$, where $e_+^2 = 1$, $e_-^2 = -1$, and $e_+ \cdot e_- = 0$, is of particular relevance for constructing conformal spaces. We note that a null basis of $\mathbb{R}^{1,1}$ is composed as the two vectors $\{e_0, e_\infty\}$ representing the origin $e_0 = \frac{1}{2}(e_- - e_+)$ and point at infinity $e_\infty = e_- + e_+$. The signature properties of e_+ and e_- and the fact that they are orthogonal imply that $e_0^2 = e_\infty^2 = 0$ and $e_0 \cdot e_\infty = -1$.

The conformal space for the Euclidean \mathbb{R}^n counterpart can be formed as $\mathbb{ME}^n \equiv \mathbb{R}^{n+1,1} = \mathbb{R}^n \oplus \mathbb{R}^{1,1}$. Thus, a Euclidean vector $\mathbf{x} \in \mathbb{R}^n$ can be embedded in the conformal space \mathbb{ME}^n as

$$X = \mathcal{C}(\mathbf{x}) = \mathbf{x} + \frac{1}{2}\mathbf{x}^2 e_\infty + e_0, \quad (3)$$

where $X \in \mathbb{ME}^n$ is called *normalized* and $\mathbf{x}^2 = \mathbf{x} \cdot \mathbf{x} = \|\mathbf{x}\|^2$. The conformal embedding (3) represents the stereographic projection of \mathbf{x} onto a projection sphere in \mathbb{ME}^n . Additionally, the embedding (3) is homogeneous, i.e., all embedding vectors in the equivalence class $[X] = \{A \in \mathbb{R}^{n+1,1} : A = \gamma X, \gamma \in \mathbb{R} \setminus \{0\}\}$ are taken to represent the same vector \mathbf{x} .

Importantly, given the conformal embedding X and some $Y = \mathbf{y} + \frac{1}{2}\mathbf{y}^2 e_\infty + e_0$, the scalar product of the two in the conformal space is their Euclidean distance, $X \cdot Y = -\frac{1}{2}(\mathbf{x} - \mathbf{y})^2$. This interpretation of the scalar product in the conformal space is the main motive in constructing spherical classifiers.

2.4 Spherical classifiers

One can construct hyperspherical decision surfaces using representations in the conformal space [18], as done in the work of [2]. A *normalized* hypersphere S is defined in the conformal space \mathbb{ME}^n as $S = \mathbf{c} + \frac{1}{2}(\mathbf{c}^2 - r^2) e_\infty + e_0 = C - \frac{1}{2}r^2 e_\infty$, where $\mathbf{c} = (c_1, \dots, c_n) \in \mathbb{R}^n$ is the hypersphere center embedded as $C \in \mathbb{ME}^n$, $r \in \mathbb{R}$ is the radius, and the coefficient for e_0 is set to 1. The scalar product of an embedded data point X and a hypersphere S in \mathbb{ME}^n yields

$$X \cdot S = X \cdot C - \frac{1}{2}r^2 X \cdot e_\infty = -\frac{1}{2}(\mathbf{x} - \mathbf{c})^2 + \frac{1}{2}r^2. \quad (4)$$

Observing that $X \cdot S = 0 \iff |\mathbf{x} - \mathbf{c}| = r$, we conclude that the scalar product determines where the input vector is relative to the hypersphere, i.e., inside if it is positive, on the surface if it is zero, or outside if it is negative.

Such a spherical classifier is the hypersphere neuron proposed in [1], where it has been demonstrated that by embedding both a data vector $\mathbf{x} \in \mathbb{R}^n$ and the hypersphere $S \in \mathbb{ME}^n$ in \mathbb{R}^{n+2} as

$$\mathbf{X} = (x_1, \dots, x_n, -1, -\frac{1}{2}\mathbf{x}^2) \in \mathbb{R}^{n+2}, \quad \mathbf{S} = (c_1, \dots, c_n, \frac{1}{2}(\mathbf{c}^2 - r^2), 1) \in \mathbb{R}^{n+2}, \quad (5)$$

the scalar product in the conformal space \mathbb{ME}^n can be computed in the isomorphic \mathbb{R}^{n+2} since

$$\mathbf{X} \cdot \mathbf{S} = \mathbf{x} \cdot \mathbf{c} - \frac{1}{2}(\mathbf{c}^2 - r^2) - \frac{1}{2}\mathbf{x}^2 = -\frac{1}{2}(\mathbf{x} - \mathbf{c})^2 + \frac{1}{2}r^2 = X \cdot S. \quad (6)$$

This result enables the implementation of a hypersphere neuron in \mathbb{ME}^n using the standard dot product in \mathbb{R}^{n+2} . The hypersphere vector components are treated as independent learnable parameters during training. Thus, a spherical classifier effectively learns *non-normalized* hyperspheres (parameter vectors) of the form $\tilde{\mathbf{S}} = (s_1, \dots, s_{n+2}) \in \mathbb{R}^{n+2}$. Due to the homogeneity of the hypersphere representation, both normalized and non-normalized hyperspheres represent the same decision surface.

Importantly, since a hypersphere can be seen as a generalization of a hyperplane, the standard neuron can be considered as a special case of the hypersphere neuron. Stacking multiple hypersphere neurons in a feed-forward network results in a multilayer hypersphere perceptron (MLHP), which was shown to outperform the standard MLP for some classification tasks in [3]. However, its application to point sets was not discussed. This motivated the work in [4] on the geometric neuron. The geometric neuron learned parameters are shown to be a combination of hypersphere neurons, i.e., spherical classifiers. This was demonstrated as the result of performing the conformal embedding of a point set

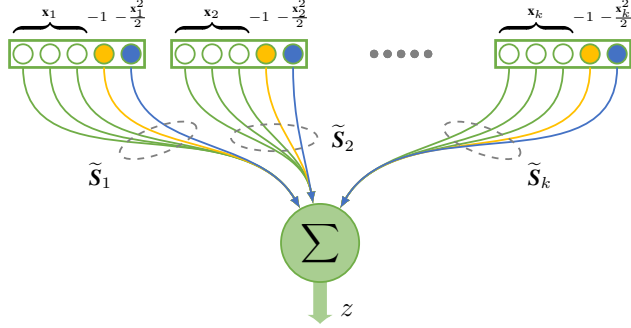


Figure 1: The geometric neuron as a generalization of the hypersphere neuron for point sets as input.

input consistently with the input geometry, see Figure 1. A single geometric neuron output is thus the sum of the signed distances of k input points to k learned hyperspheres

$$z = \sum_{k=1}^N \gamma_k \mathbf{X}_k^\top \mathbf{S}_k, \quad (7)$$

where $z \in \mathbb{R}$, $\mathbf{X}_k \in \mathbb{R}^5$ is a properly embedded 3D input point, $\gamma_k \in \mathbb{R}$ is the scale factor, i.e., the last element of the learned parameter vector $\tilde{\mathbf{S}}_k$, and $\mathbf{S}_k = \tilde{\mathbf{S}}_k / \gamma_k \in \mathbb{R}^5$ are the corresponding normalized learned parameters (hyperspheres). We refer to the original work for a more detailed description. Furthermore, [4] demonstrates that the geometric neuron activations are isometric in 3D, i.e., rotating the input is equivalent to rotating the hypersphere neurons in the opposite direction. This result is a necessary condition to consider rigid body transformation equivariance properties of models constructed with geometric neurons and forms the basis for our methodology.

In the following sections, we use the same notation for a 3D rotation \mathbf{R} represented in the Euclidean space \mathbb{R}^3 , the homogeneous (projective) space $P(\mathbb{R}^3)$, and $\mathbb{ME}^3 \cong \mathbb{R}^5$, depending on the context. This is possible since we can add the required number of 1 to the diagonal of the original rotation matrix without changing the transformation representation.

3 Method

To build a 3D steerable model, we perform the following steps: We first train an MLGP model [4], which has spherical classifiers as atomic elements. After optimizing the model parameters, we will “freeze” them and transform according to the 3D steerability constraint we derive. By combining the resulting parameters in filter banks and adding interpolation coefficients as learnable parameters, we will thus create a steerable model.

3.1 Fully steerable 3D spherical neurons

In this section, we identify the conditions under which a geometric neuron as a function of its 3D input can be steered. In other words, we derive an expression that gives us the response of a *hypothetical* geometric neuron for some input, using rotated versions of the learned geometric neuron parameters. We start by considering the steerability conditions for the geometric neuron atomic parts, i.e., spherical classifiers acting on input \mathbf{X} as in (7), i.e., $f(\mathbf{X}) = \mathbf{X}^\top \mathbf{S}$, where \mathbf{X} and \mathbf{S} are embedded in $\mathbb{ME}^3 \cong \mathbb{R}^5$ according to (5). Since the geometric neuron output is a linear combination of these functions, as per (7), we will use the identified conditions to build a steerable feed-forward network by reassembling modified atomic parts.

3.1.1 Basis construction

To formulate a steerability constraint for a spherical classifier (sphere), first, we need to determine the minimum number of basis functions, i.e., the number of terms M in (2).

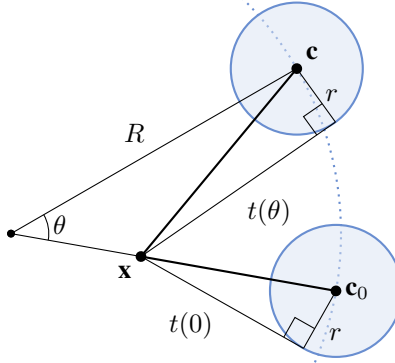


Figure 2: The effect of rotation on the spherical classifier activation in 2D; $t(\theta)$ is the tangent length.

Consider the 2D case first. Assume a 2D spherical classifier \mathbf{S} with center \mathbf{c} ($R := \|\mathbf{c}\|$) and radius r (5), and a point \mathbf{x} lying outside of it. According to [4], the scalar product $\mathbf{X}^\top \mathbf{S}$ is proportional to the squared tangent length, see Figure 2. Thus, by means of (6), some basic algebraic manipulations, and the cosine theorem, we have

$$\mathbf{X}^\top \mathbf{S} = -\frac{1}{2}(\|\mathbf{x} - \mathbf{c}\|^2 - r^2) = -\frac{1}{2}(R^2 - 2R\|\mathbf{x}\| \cos(\theta) + \|\mathbf{x}\|^2 - r^2), \quad (8)$$

where θ is the angle formed by the vectors \mathbf{x} and \mathbf{c} . Note that if the point happens to lie inside or on the circle, this does not change (8), only the sign of the result, as the right-hand side becomes positive. From the obtained expression, we observe that the effect of rotating a spherical unit, i.e., a circle, on the value of its activation for some input point is determined by the spherical harmonics up to the first order ($N = 1$), i.e., $\cos(\theta)$, and some DC-component.

In 3D, consider a rotation in the plane spanned by the center of the sphere and the point. In this case, we will reduce the problem to 2D, and the scalar product can be found as we showed above (8). In the general case, the sphere center rotates in a plane that does not contain the point, as demonstrated in Figure 3. Assume without loss of generality $\mathbf{c}_0 = (R, 0, 0)$ and $\mathbf{x} = (x, 0, z)$, i.e., the point is located with distance z to the plane. The sphere (\mathbf{c}_0, r) is rotated about the z -axis with angle θ into the sphere (\mathbf{c}, r) . We now get for the squared scaled tangent through \mathbf{x} (i.e., the scalar product between the \mathbb{R}^5 embeddings \mathbf{X} and \mathbf{S})

$$\mathbf{X}^\top \mathbf{S} = -\frac{1}{2}(z^2 + R^2 + x^2 - r^2 - 2Rx \cos \theta) \quad (9)$$

with the following computations (note that $\mathbf{c} = (R \cos \theta, R \sin \theta, 0)$ and we assume in the first equality that the point is outside of the sphere)

$$\begin{aligned} -2\mathbf{X}^\top \mathbf{S} &= \|\mathbf{x} - \mathbf{c}\|^2 - r^2 = \|(x - R \cos \theta, -R \sin \theta, z)\|^2 - r^2 \\ &= (x - R \cos \theta)^2 + R^2 \sin^2 \theta + z^2 - r^2 \\ &= x^2 - 2Rx \cos \theta + R^2 \cos^2 \theta + R^2 \sin^2 \theta + z^2 - r^2, \end{aligned}$$

and (9) follows. Thus, we only get the additional term z^2 compared to (8) and we still need only the spherical harmonics of order ≤ 1 to determine the effect of rotation on the 3D spherical classifier activation. Thus, the classifier is equivariant with respect to rotations. Following the result of Theorem 4 in [6] and using $N = 1$, we have that $M = (N + 1)^2 = 4$ basis functions suffice in (2).

In consistence with [6], we thus select four rotated versions of the function $f(\mathbf{X})$, as the basis functions. The rotations $\{\mathbf{R}_j\}_{j=1}^4$ must be chosen to satisfy the condition (b) in Theorem 4 ([6]). Therefore, we transform $f(\mathbf{X})$ such that the resulting four spheres are spaced in three dimensions equally, that is, form a regular tetrahedron with the vertices $(1, 1, 1)$, $(1, -1, -1)$, $(-1, 1, -1)$, and $(-1, -1, 1)$, as shown in Figure 4 b). We stack the homogeneous coordinates of the tetrahedron vertices \mathbf{m}_j in a matrix column-wise (scaled by $1/2$) to get the orthogonal matrix

$$\mathbf{M} = [\mathbf{m}_1 \quad \mathbf{m}_2 \quad \mathbf{m}_3 \quad \mathbf{m}_4] = \frac{1}{2} \begin{bmatrix} 1 & 1 & -1 & -1 \\ 1 & -1 & 1 & -1 \\ 1 & -1 & -1 & 1 \\ 1 & 1 & 1 & 1 \end{bmatrix}. \quad (10)$$

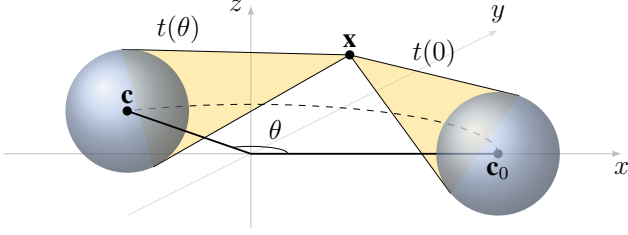


Figure 3: The effect of rotation on the spherical classifier activation in 3D; $t(\theta)$ is the tangent length.

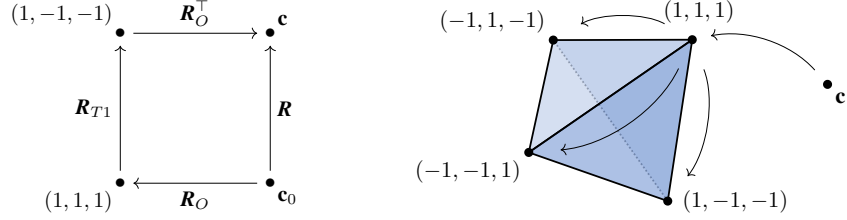


Figure 4: a) A rotation from \mathbf{c}_0 to \mathbf{c} described by a tetrahedron rotation. b) A regular tetrahedron.

We will use this matrix operator \mathbf{M} to compute the linear coefficients in the vector space generated by the vertices of the regular tetrahedron [19]. This will be necessary to find the appropriate interpolation functions and formulate the steerability constraint in Section 3.1.3.

3.1.2 Spherical filter banks

The four rotated versions of the function $f(\mathbf{X})$ will constitute the basis functions that we call a spherical filter bank. To construct this filter bank, we choose the following convention. The originally learned spherical classifier $\mathbf{S} = f$ is first rotated to $(1, 1, 1)$ (see Figure 4 b)) with the corresponding transformation denoted as \mathbf{R}_O . Next, we rotate the transformed sphere into the other three vertices of the regular tetrahedron described in Section 3.1.1 and transform back to the original coordinate system. The resulting filter bank for one spherical classifier is thus composed as the following matrix:

$$B(\mathbf{S}) = \begin{bmatrix} \mathbf{R}_O^\top \mathbf{R}_{T0} \mathbf{R}_O \mathbf{S} \\ \mathbf{R}_O^\top \mathbf{R}_{T1} \mathbf{R}_O \mathbf{S} \\ \mathbf{R}_O^\top \mathbf{R}_{T2} \mathbf{R}_O \mathbf{S} \\ \mathbf{R}_O^\top \mathbf{R}_{T3} \mathbf{R}_O \mathbf{S} \end{bmatrix}, \quad (11)$$

where \mathbf{R}_{Tj} is the rotation isomorphism in \mathbb{R}^5 corresponding to a 3D rotation from $(1, 1, 1)$ to the vertex $j + 1$ of the regular tetrahedron. Therefore, $\mathbf{R}_{T0} = \mathbf{I}_5$.

3.1.3 3D steerability constraint

The steerability constraint can be formulated as follows. For an arbitrary orientation \mathbf{R} applied to the input of the function $f(\mathbf{X})$, we want the output of the spherical filter bank $B(\mathbf{S})$ in (11) to be interpolated with $v_j(\mathbf{R})$ such that the response is equal to the original function output, i.e.,

$$f(\mathbf{X}) = f^{\mathbf{R}}(\mathbf{R}\mathbf{X}) = \sum_{j=1}^M v_j(\mathbf{R}) f^{\mathbf{R}_j}(\mathbf{R}\mathbf{X}) = (v(\mathbf{R}) \otimes \mathbf{R}\mathbf{X})^\top B(\mathbf{S}), \quad (12)$$

where $\mathbf{X} \in \mathbb{R}^5$ is a single, appropriately embedded, 3D point, $v(\mathbf{R}) \in \mathbb{R}^4$ is a vector of the interpolation coefficients, and \otimes denotes the Kronecker product [20].

The coefficients $v(\mathbf{R})$ should conform to the basis function construction (condition (b) in Theorem 4 [6]), which is why they are computed with \mathbf{M} defined in (10). Given $\mathbf{X} \in \mathbb{R}^5$ as input and an unknown rotation \mathbf{R} acting on it, the steering equation (12) implies

$$(v(\mathbf{R}) \otimes \mathbf{R}\mathbf{X})^\top B(\mathbf{S}) = (v(\mathbf{I}) \otimes \mathbf{X})^\top B(\mathbf{S}). \quad (13)$$

Given a tetrahedron rotation, e.g., \mathbf{R}_{T1} , as shown in the diagram in Figure 4 a), we can define the unknown rotation accordingly as $\mathbf{R} = \mathbf{R}_O^\top \mathbf{R}_{T1} \mathbf{R}_O$. In this case, it is easy to see that to satisfy the constraint (13), $v(\mathbf{R})$ must be $(0, 1, 0, 0)$, i.e., the second filter in the filter bank $B(\mathbf{S})$ must be chosen. This can be achieved by transforming a constant vector $\mathbf{m}_1 = (\frac{1}{2}, \frac{1}{2}, \frac{1}{2}, \frac{1}{2})$ by rotation \mathbf{R}_{T1} and multiplying it by the basis matrix \mathbf{M} as follows:

$$v(\mathbf{R}) = \mathbf{M}^\top (\mathbf{R}_{T1} \mathbf{m}_1) = \mathbf{M}^\top \left(\frac{1}{2}, -\frac{1}{2}, -\frac{1}{2}, \frac{1}{2} \right) = (0, 1, 0, 0). \quad (14)$$

Note that, in general, a geometric neuron (7) takes a *set* of embedded points as input. Therefore, with the setup above, \mathbf{R} will be different for each input shape point k if the same v is used for all k , which contradicts that the shape is transformed by a rigid body motion, i.e., the same \mathbf{R}_B for all k . Thus, we need to consider a suitable vector v^k for each input shape point k , such that the resulting \mathbf{R}_B is the same for all k . This can be achieved recalling how we construct the basis functions in the spherical filter bank (11): we need to consider the respective initial rotation \mathbf{R}_O^k . The desired interpolation coefficients v^k are thus computed as

$$v^k(\mathbf{R}_B) = \mathbf{M}^\top (\mathbf{R}_O^k \mathbf{R}_B \mathbf{R}_O^{k\top} \mathbf{m}_1). \quad (15)$$

The resulting $v^k(\mathbf{R}_B)$ interpolate the responses of the tetrahedron-copies of the originally learned sphere \mathbf{S}_k to replace the rotated sphere.

We can now define the steerability constraint for a geometric neuron that takes a set of N embedded points $\{\mathbf{X}_k\}_k$ as input by plugging (12) into (7):

$$f^{\mathbf{R}}(\mathbf{R}\mathbf{X}) = \sum_{k=1}^N \gamma_k f^{k\mathbf{R}}(\mathbf{R}\mathbf{X}_k) = \sum_{k=1}^N \gamma_k (v^k(\mathbf{R}) \otimes \mathbf{R}\mathbf{X}_k)^\top B(\mathbf{S}_k). \quad (16)$$

4 Experiments

We perform two types of experiments to confirm our findings presented in Section 3. We conduct all experiments on a GTX 1050 Ti GPU, and it takes less than a minute per run.

4.1 Synthetic point set

Following the experiments reported in [5, 16, 4], we use the synthetic point set of eight 3D Tetris shapes consisting of four points each. The dataset is:

```
chiral_shape_1: [(0, 0, 0), (0, 0, 1), (1, 0, 0), (1, 1, 0)],
chiral_shape_2: [(0, 0, 0), (0, 0, 1), (1, 0, 0), (1, -1, 0)],
square: [(0, 0, 0), (1, 0, 0), (0, 1, 0), (1, 1, 0)],
line: [(0, 0, 0), (0, 0, 1), (0, 0, 2), (0, 0, 3)],
corner: [(0, 0, 0), (0, 0, 1), (0, 1, 0), (1, 0, 0)],
L: [(0, 0, 0), (0, 0, 1), (0, 0, 2), (0, 1, 0)],
T: [(0, 0, 0), (0, 0, 1), (0, 0, 2), (0, 1, 1)],
zigzag: [(0, 0, 0), (1, 0, 0), (1, 1, 0), (2, 1, 0)].
```

4.2 Steerable model construction

We first train a two-layer MLGP model [4], whose hidden layer consists of geometric neurons and whose output layer consists of hypersphere neurons, to *perfectly* classify the eight synthetic 3D shapes that are in the canonical orientation, as described in Section 4.1. Since the architecture choice is not the objective of the experiments, we use only one configuration with five hidden units throughout the experiments. Similar to [4], we do not use any activation function in the hidden layer due to the non-linearity of the conformal embedding. The final layer is equipped with the softmax activation function. We implement the MLGP model in PyTorch [21]. We keep the default parameter initialization for PyTorch linear layers. We train the model for 2000 epochs by minimizing the cross-entropy loss function. We use the Adam optimizer [22] with the default hyperparameters (the learning rate is 0.001). We call this model the *ancestor* MLGP.

We then “freeze” the trained parameters and construct a steerable model. Note that we form steerable units only in the hidden layer and keep the output, i.e., classification, layer hypersphere neurons as

Table 1: Known rotation experiment: the steerable model classification accuracy of the 8 distorted rotated shapes and the L1 distance to the ground truth activations (mean and std over 1000 runs).

Transformed data noise level (a)	L1 distance	Accuracy, %
0.00	0.00 ± 0.00	100.0 ± 0.0
0.05	0.33 ± 0.05	100.0 ± 0.0
0.10	0.66 ± 0.10	100.0 ± 0.0
0.20	1.32 ± 0.19	100.0 ± 0.4
0.30	2.00 ± 0.31	99.7 ± 1.9
0.50	3.33 ± 0.48	94.9 ± 7.7

they are. The steerable units are formed from the corresponding frozen parameters as the filter banks, according to (11), and they are fixed, i.e., not being learned.

The only learnable parameters of this constructed steerable model are interpolation coefficients $v^k(\mathbf{R}_B) \in \mathbb{R}^4$ defined in (15), where k indexes the learned hidden layer parameters (spheres) in the ancestor MLGP model. But since the only variables in (15) are the parameters of the unknown rotation \mathbf{R}_B acting on the input, we can directly optimize them if they are unknown. We select the *axis-angle* rotation representation because it has only three parameters — the three coordinates of the rotation axis scaled by the rotation angle.

We propose the following basic recipe to create a steerable model: Train the ancestor MLGP → Fix the learned parameters → Transform the hidden unit parameters into filter banks (11) → Add the interpolation coefficients v^k as learnable parameters to fulfill (16) → Steerable spherical classifier.

4.3 Known transformation experiment

Using the trained MLGP, we verify the correctness of (16). We first rotate the eight shapes and then use this ground truth rotation to set the interpolation coefficients of the constructed steerable model according to (15). Our intuition is that if the steerability constraint (16) is correct, then, given the transformed point set, the activations of the steerable units in the steerable model will be equal to the activations of the geometric neurons in the ancestor MLGP model fed with the point set in the canonical orientation. Hence, the classification accuracies of the two models on the respective two datasets should be equal.

We run this experiment 1000 times. Each time, we generate a random rotation and apply it to the original point set. We use these rotation parameters to create a steerable model and evaluate it on the transformed point set. To verify the stability of the steerable unit activations, we add uniform noise to the transformed points, $\mathbf{n} \sim U(-a, a)$. We also compare the hidden unit activations of the two models by computing the L1 distance. For convenience, we call the activations of the ancestor MLGP fed with the canonical training set, which it has learned to classify perfectly, ground truth activations. We summarize the results in Table 1.

4.4 Adaptive rotation experiment

Adaptivity in this context means that we feed some rotation information into the system. For example, this information can come from another network branch that performs regression on the rotation, or from a dynamical model as in tracking. In either case, we cannot assume that the rotation is absolutely accurate, unlike the experiment in Section 4.3. Therefore, we check the stability with respect to the noise in the rotation. Same as before, we exploit the MLGP trained on the point set in the canonical orientation, as described in Section 4.3, to build the steerable model.

At each experiment run, we randomly select one shape and apply a random rotation, \mathbf{R}_{GT} , to it. We then perturb this ground truth rotation by varying the rotation angle. We achieve this by sampling the rotation angle from a Gaussian distribution with $\sigma = \pi/18$ and various means, constructing a rotation of this sampled angle about a random axis, $\mathbf{R}_{\text{noise}}$, and multiplying with the ground truth: $\mathbf{R}_{\text{init}} = \mathbf{R}_{\text{noise}} \mathbf{R}_{\text{GT}}$. We use the resulting rotation \mathbf{R}_{init} in the axis-angle representation to initialize the steerable model parameters.

Further, we perform the optimization of the rotation vector parameters, which we call *online* optimization. Since we are at inference time, we do not have access to the labels. Thus, we need to select a loss

Table 2: Adaptive rotation experiment: the steerable model classification accuracy (mean over 1000 runs) for a randomly chosen rotated shape and the L1 distance to the ground truth softmax output (mean and std over 1000 runs) before and after online optimization.

Initial rotation noise mean	Initial L1	Final L1	Initial accuracy, %	Final accuracy, %
0	0.007 ± 0.033	0.007 ± 0.031	99.9	99.9
$\pi/36$	0.009 ± 0.038	0.007 ± 0.032	99.8	99.9
$\pi/18$	0.013 ± 0.046	0.007 ± 0.044	99.8	99.8
$\pi/12$	0.025 ± 0.080	0.012 ± 0.082	99.2	99.3
$\pi/6$	0.106 ± 0.205	0.064 ± 0.232	93.6	94.1

based on the consistency of the output. Here, we choose the entropy, i.e., $\mathcal{L}(\mathbf{p}) = -\sum_{i=1}^K p_i \log(p_i)$, where $\mathbf{p} \in \mathbb{R}^K$ is the softmax output of the model. Our intuition is that by minimizing the entropy in the output with respect to the steerable model parameters, we effectively force the model to produce a more confident prediction, i.e., one that is close to the Dirac delta. For this optimization procedure, we use Adam with learning rate equal to 0.01, and set the number of epochs to 300.

Note that at each run, we provide the model with only one transformed shape, which implies that the accuracy per experiment is binary, i.e., the shape is either recognized (1) or misclassified (0). To verify the usefulness of the proposed online optimization method, we compare the model classification accuracy before and after optimization. Also, we compute the L1 distance from the steerable model softmax output to softmax output of the ancestor MLGP model fed with the shapes in the canonical orientation, i.e., the *ground truth output* (similar to what we did in Section 4.3). The results for this experiment are presented in Table 2.

5 Discussion

Enabled by the understanding the complete geometry of the spherical classifiers [1, 2, 4], we show in Section 3 that we only need the spherical harmonics of order up to $N = 1$ to determine the effect of rotation on the activations in 3D. Using this result, we derive a novel 3D steerability constraint (16).

The conducted experiment in Section 4.3 shows that the derived constraint is correct since the constructed steerable model produces accurate predictions for the rotated shapes, provided that the rotation is known. From Table 1, we can see that both the model classification error and the L1 distance to the respective hidden unit activations of the ancestor MLGP model moderately increase with the level of noise in the input data, which is a clear indication of the robustness of the classifier.

The experiment presented in Section 4.4 considers a more realistic setting, where the rotation applied to the input is not known exactly but inaccurately estimated. However, unlike the first experiment, we perform an optimization to improve the initial steerable model prediction. The only three parameters of the model — the axis-angle representation of the *unknown* external rotation — determining the interpolation coefficients v^k , are optimized by minimizing the entropy in the model output. As displayed in Table 2, our steerable model, even prior to the optimization, produces rotation-invariant predictions for the transformed shapes. The proposed online optimization results in the decrease of the L1 distance to the ancestor MLGP softmax output values and improves the model classification accuracy, see Table 2.

The power of our approach lies in the geometric explainability inherent to the spherical units that constitute our model. Seemingly complicated conformal algebra operations have a surprisingly straightforward interpretation in the Euclidean space and allow us to build a steerable feed-forward neural network with a purely geometric motivation and no “black-box” routines. The steerable spherical neurons discussed in our work can be employed in other architectures, e.g., CNNs, and therefore, the equivariance to transformations beyond rotation can be considered.

Acknowledgments and Disclosure of Funding

This work was partially supported by the Wallenberg AI, Autonomous Systems and Software Program (WASP), by the Swedish Research Council through a grant for the project Algebraically Constrained Convolutional Networks for Sparse Image Data (2018-04673), and by the Centre for Industrial Information Technology (CENIIT).

References

- [1] V. Banarer, C. Perwass, and G. Sommer, “The hypersphere neuron,” in *ESANN*, pp. 469–474, 2003.
- [2] C. Perwass, V. Banarer, and G. Sommer, “Spherical decision surfaces using conformal modelling,” in *Joint Pattern Recognition Symposium*, pp. 9–16, Springer, 2003.
- [3] V. Banarer, C. Perwass, and G. Sommer, “Design of a multilayered feed-forward neural network using hypersphere neurons,” in *International Conference on Computer Analysis of Images and Patterns*, pp. 571–578, Springer, 2003.
- [4] P. Melnyk, M. Felsberg, and M. Wadenbäck, “Embed Me If You Can: A Geometric Perceptron,” *arXiv preprint arXiv:2006.06507*, 2020.
- [5] N. Thomas, T. Smidt, S. Kearnes, L. Yang, L. Li, K. Kohlhoff, and P. Riley, “Tensor field networks: Rotation- and translation-equivariant neural networks for 3D point clouds,” *arXiv preprint arXiv:1802.08219*, 2018.
- [6] W. T. Freeman, E. H. Adelson, *et al.*, “The design and use of steerable filters,” *IEEE Transactions on Pattern analysis and machine intelligence*, vol. 13, no. 9, pp. 891–906, 1991.
- [7] H. Knutsson, L. Haglund, H. Barman, and G. Granlund, “A framework for anisotropic adaptive filtering and analysis of image sequences and volumes,” in *[Proceedings] ICASSP-92: 1992 IEEE International Conference on Acoustics, Speech, and Signal Processing*, vol. 3, pp. 469–472 vol.3, 1992.
- [8] L. Van Gool, T. Moons, E. Pauwels, and A. Oosterlinck, “Vision and Lie’s approach to invariance,” *Image and Vision Computing*, vol. 13, no. 4, pp. 259–277, 1995.
- [9] M. Reisert, “Group integration techniques in pattern analysis: a kernel view,” 01 2008.
- [10] B. Anderson, T. S. Hy, and R. Kondor, “Cormorant: Covariant molecular neural networks,” in *Advances in Neural Information Processing Systems*, pp. 14510–14519, 2019.
- [11] D. Marcos, M. Volpi, N. Komodakis, and D. Tuia, “Rotation Equivariant Vector Field Networks,” in *Proceedings of the IEEE International Conference on Computer Vision (ICCV)*, Oct 2017.
- [12] R. Kondor, Z. Lin, and S. Trivedi, “Clebsch–Gordan Nets: a Fully Fourier Space Spherical Convolutional Neural Network,” in *Advances in Neural Information Processing Systems* (S. Bengio, H. Wallach, H. Larochelle, K. Grauman, N. Cesa-Bianchi, and R. Garnett, eds.), vol. 31, Curran Associates, Inc., 2018.
- [13] T. S. Cohen and M. Welling, “Steerable CNNs,” *arXiv preprint arXiv:1612.08498*, 2016.
- [14] M. Weiler, F. A. Hamprecht, and M. Storath, “Learning steerable filters for rotation equivariant CNNs,” in *Proceedings of the IEEE Conference on Computer Vision and Pattern Recognition*, pp. 849–858, 2018.
- [15] M. Weiler and G. Cesa, “General $E(2)$ -Equivariant Steerable CNNs,” *arXiv preprint arXiv:1911.08251*, 2019.
- [16] M. Weiler, M. Geiger, M. Welling, W. Boomsma, and T. S. Cohen, “3D steerable CNNs: Learning rotationally equivariant features in volumetric data,” in *Advances in Neural Information Processing Systems*, pp. 10381–10392, 2018.
- [17] H. Li, D. Hestenes, and A. Rockwood, “Generalized homogeneous coordinates for computational geometry,” in *Geometric Computing with Clifford Algebras*, pp. 27–59, Springer, 2001.
- [18] H. Li, D. Hestenes, and A. Rockwood, “A universal model for conformal geometries of Euclidean, spherical and double-hyperbolic spaces,” in *Geometric computing with Clifford algebras*, pp. 77–104, Springer, 2001.
- [19] G. Granlund and H. Knutsson, eds., *Signal Processing for Computer Vision*. Dordrecht: Kluwer, 1995.
- [20] R. A. Horn and C. R. Johnson, *Topics in Matrix Analysis*. New York, NY, USA: Cambridge University Press, 1991.
- [21] A. Paszke, S. Gross, F. Massa, A. Lerer, J. Bradbury, G. Chanan, T. Killeen, Z. Lin, N. Gimelshein, L. Antiga, *et al.*, “Pytorch: An imperative style, high-performance deep learning library,” in *Advances in Neural Information Processing Systems*, pp. 8024–8035, 2019.
- [22] D. P. Kingma and J. Ba, “Adam: A method for stochastic optimization,” in *Proceedings of the International Conference on Learning Representations (ICLR)*, 2015.